

## Article

# The Influence of Spatial Heterogeneity of Urban Green Space on Surface Temperature

Mengru Zhang <sup>1</sup>, Jianguo Wang <sup>1</sup> and Fei Zhang <sup>2,\*</sup> 

<sup>1</sup> College of Geography and Remote Sensing Sciences, Xinjiang University, Urumqi 830017, China; zhangmr981114@163.com (M.Z.); jianguowang@ksu.edu.cn (J.W.)

<sup>2</sup> College of Geography and Environmental Sciences, Zhejiang Normal University, Jinhua 321004, China

\* Correspondence: zhangfei3s@163.com or zhangfei3s@zjnu.edu.cn

**Abstract:** Urban green space (UGS) has been recognized as a key factor in enhancing the urban ecosystem balance, particularly in arid areas. It is often considered an effective means to mitigate the urban heat island (UHI) effect. In this study, the reference comparison method was utilized to optimize the process of nighttime lighting data; the random forest classification method was employed to extract UGS data; and the radiative transfer method was applied in land surface temperature (LST) inversion. Additionally, moving window analysis was conducted to assess the robustness of the results. The objective of this research was to analyze the spatial distribution characteristics of UGS and LST and to explore their bivariate local spatial autocorrelations by calculating four landscape metrics, including the aggregation index (AI), edge density (ED), patch density (PD), and area-weighted mean shape index (Shape\_am). It was found that the distribution of UGS in the study area was uneven, with higher temperatures in the eastern and western regions and lower temperatures in the central and southern regions. The results also revealed that ED, PD, and Shape\_am were negatively correlated with LST, with correlation coefficients being  $-0.469$ ,  $-0.388$ , and  $-0.411$ , respectively, indicating that UGS in these regions were more effective in terms of cooling effect. Conversely, AI was found to be positively correlated with LST (Moran' I index of 0.449), indicating that surface temperatures were relatively higher in regions of high aggregation. In essence, the fragmented, complex, and evenly distributed green patches in the study area provided a better cooling effect. These findings should persuade decision makers and municipal planners to allocate more UGS in cities for UHI alleviation to improve quality of life and enhance recreational opportunities.

**Keywords:** urban green space (UGS); land surface temperature (LST); Gaofen-2; thermal comfort; bivariate local spatial autocorrelation



**Citation:** Zhang, M.; Wang, J.; Zhang, F. The Influence of Spatial Heterogeneity of Urban Green Space on Surface Temperature. *Forests* **2024**, *15*, 878. <https://doi.org/10.3390/f15050878>

Academic Editor: Paloma Cariñanos

Received: 16 April 2024

Revised: 13 May 2024

Accepted: 15 May 2024

Published: 17 May 2024



**Copyright:** © 2024 by the authors. Licensee MDPI, Basel, Switzerland. This article is an open access article distributed under the terms and conditions of the Creative Commons Attribution (CC BY) license (<https://creativecommons.org/licenses/by/4.0/>).

## 1. Introduction

The United Nations 2030 Agenda for Sustainable Development has proposed 17 Sustainable Development Goals (SDGs), of which SDG 11 is “to build inclusive, safe, resilient and sustainable cities and human settlements” [1]. This goal underscores the global and national focus on sustainable urban development, which was intensified by rising personal incomes and public demand for higher-quality living environments. Consequently, the Chinese government escalated the requirements for living environments of residents in its pursuit of ecological civilization [2]. Urban green space (UGS) is a vital component of the urban environment, playing significant roles in the ecological and social realms [3]. Therefore, rationalizing the allocation of UGS to enhance thermal comfort in urban areas has become a pressing issue.

Since the 20th century, the rapid development of cities has brought many ecological and environmental problems, among which the urban heat environment is particularly prominent. Large amounts of construction, industrial emissions, and other human activities lead to a continuous increase in surface temperature, causing cities to be hotter than

surrounding zones. This phenomenon is known as the urban heat island (UHI) effect [4]. In general, two types of UHI are recognized: the air temperature UHI, which affects atmospheric conditions, and the surface temperature UHI, sometimes referred to as the surface urban heat island (SUHI), which impacts the temperatures of urban surfaces [5]. Air temperature UHI can be extracted from infrared remote sensing images with land surface temperature (LST) and has been extensively utilized to study the UHI phenomenon [6]. LST threatens the urban ecological environment, and there are natural disasters such as heat waves and floods, and it is increasingly used to study UHI. A number of researchers have indicated that UGSs perform a very valuable function in improving urban thermal environment problems [7–9] and has important ecological landscape and health value for cities and residents, not only improving air quality and reducing noise pollution and extreme weather impacts on people’s lives, but also reducing stress on humans by controlling the development of UHI. It can improve air quality, reduce the impact of noise pollution and extreme weather on people’s lives, as well as promote psychological health by reducing stress, thus making residents more comfortable. With the growing urbanization and the increasing expectation to have a higher quality of life in urban environments, the impact of UGS on human settlements has proven to be increasingly evident and has become a key enabling aspect for all governments and societies in urban planning. However, different green space patterns have different relationships with urban temperature, and exploring their patterns and distributions is important for planners to optimize urban patterns in the future.

Recent studies have consistently highlighted the crucial role of UGS in mitigating UHI effects [10–12]. These studies illustrate various mechanisms, through which UGSs lower LST, such as shading and evapotranspiration [13,14]. Despite the limited availability of land for greening in urban planning, more attention has been given to the effect of the spatial configuration of green space on LST, aiming to maximize cooling benefits by modifying its spatial distribution. It has been demonstrated that the spatial configuration of green space significantly influences LST [11,15], with the area, shape, and type of UGS being crucial factors. While some studies indicate a strong cooling effect related to the proportion of area covered by UGS [8,16], there is no consensus on the impact of UGS shape and type on temperature, potentially due to variations in study areas, data spatial resolution, etc. [6,17,18]. Furthermore, comparative studies across different urban settings have shown that the effectiveness of UGS in reducing LST varies significantly and depends on the local climatic conditions, urban morphology, and vegetation types [19,20]. However, while there is a growing understanding of these processes, significant gaps remain in specific areas such as semi-arid regions, where unique climatic challenges exacerbate the UHI effect [21]. Moreover, the impact of UGS configuration—such as the size, shape, and connectivity of green spaces—on urban thermal comfort is still not fully understood, with studies reporting mixed outcomes based on the spatial resolution of the data used and the methodological approaches employed [22,23].

This study delineates the influence of various configurations of UGS on LST, providing crucial insights for strategic UGS planning and optimization within urban settings. Notably, variations in the geographic scope of study areas, analytical scales, and the resolution of the data employed can significantly affect temperature outcomes. A review of the literature highlights a significant lack of empirical investigations into arid regions [24], which face unique challenges such as acute water shortages that could be exacerbated by global warming [25]. These gaps underscore the need for a comprehensive exploration of the direct interactions between UGS and LST. Additionally, variations in findings regarding the associations between landscape metrics and LST across different studies call for comparative analyses with other regional case studies.

This investigation aims to provide a robust scientific basis for UGS optimization by addressing pivotal questions including the following: (1) What are the spatial distributions of UGS landscape patterns in different regions? (2) How does LST vary spatially across these regions? (3) What are the differences in the correlation between the spatial distribution of

UGS and LST in different regions? To our knowledge, this is the inaugural study in Urumqi employing GIS technology and spatial metrics to analyze the correlation between UGS and LST. The outcomes of this analysis are anticipated to furnish the governmental policy makers and urban planners with enhanced understanding of the UGS spatial patterns and facilitate more profound investigations into the correlation between UGS and LST across the entire urban community.

## 2. Materials and Methods

### 2.1. Study Area

Urumqi, the capital of Xinjiang, is situated in the northwest border of China, encompassed by coordinates ranging from 86°37'33" to 88°58'24" E and 42°45'32" to 45°00'00" N. It is enclosed by mountain ranges on three sides, and the city boasts an average altitude of 800 m (Figure 1). Characterized by a mid-temperate semi-arid continental climate, Urumqi is distinguished as the city farthest from any ocean globally, receiving an average annual precipitation of only 236 mm. According to the Köppen-Geiger climate classification system, this climatic condition categorizes Urumqi in the Cold Semi-Arid (BSk) zone. Summers exhibit high temperatures, with peak heat occurring in July and August, boasting an average temperature of 25.7 °C. Winters, on the other hand, are characterized by mild conditions, with an average temperature of −15.2 °C. This moderation is attributed to the barrier effect of the Tien Shan Mountains, which effectively entraps cold air within the basin.

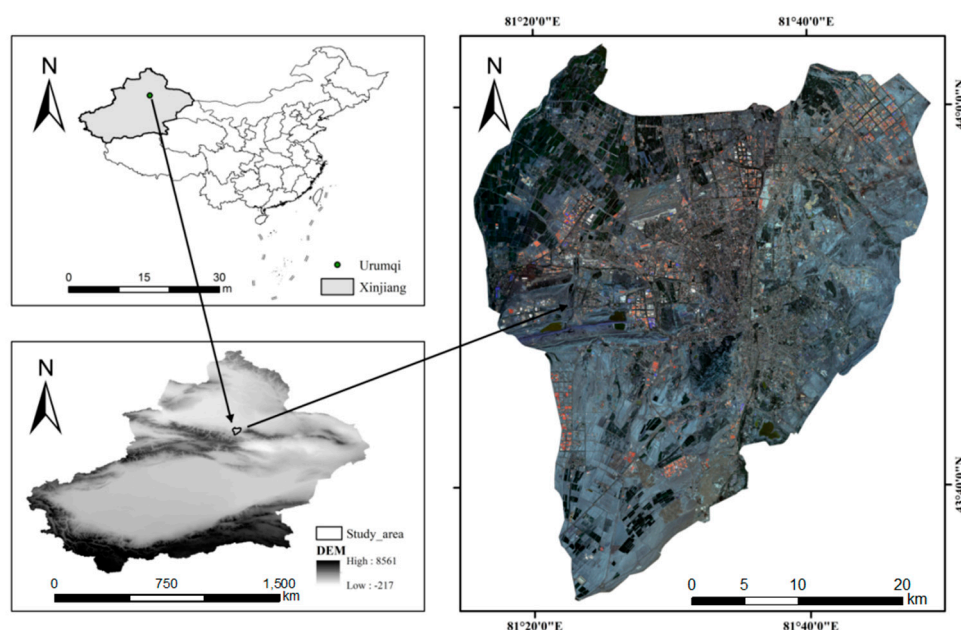


**Figure 1.** Location map of the study area.

As reported in the 2021 National Economic and Social Development Statistical Bulletin of Urumqi (<http://www.urumqi.gov.cn/fjbm/tj/tjgb/509211.htm>, accessed on 14 September 2022), the city covers an area of approximately  $1.38 \times 10^4$  km<sup>2</sup>, with the built-up area having expanded by 14.60 km<sup>2</sup> from the previous year to 536.20 km<sup>2</sup>. With a resident population of 4.05 million, Urumqi stands as Xinjiang's major urban center and the most populous and economically dynamic city in Central Asia. The UGS in Urumqi faces significant challenges due to the harsh dry climate, climate change, and rapid urban expansion, which emphasize the necessity for strategic environmental planning and management. Thus, Urumqi, the capital of the Xinjiang Uyghur Autonomous Region, is selected as the focal study area to investigate the impact of green space composition and configuration on LST.

## 2.2. Research Data

UGSs, distributed within urban areas, are the focus of this paper. For the precise definition of urban built-up areas, nighttime light data from the Lujia-1 (LJ1-01) satellite [26,27], developed by Wuhan University, were employed. As the world's first satellite dedicated to luminescence remote sensing, LJ1-01 has been widely validated to monitor and extract economic activities in urban built-up areas. Data acquired on 30 October 2018, with a spatial resolution of 130 m, were utilized to define urban built-up areas accurately.

The Gaofen-2 (GF-2) satellite, launched by China, represents a significant advancement in civil optical remote sensing technology. With a spatial resolution exceeding 1 m, it is the highest resolution civil remote sensing satellite developed by China to date. Its extensive observation area and long operational lifespan [28] make GF-2 an exemplary data source for urban studies [29]. In this research, GF-2 PMS images captured on 21 July 2021 and 1 August 2021 were used to comprehensively cover the designated study area. The image processing was meticulously executed using ENVI 5.3 software, which involved several critical stages. Radiometric calibration was performed with settings adjusted to "Radiance", converting raw data to accurate radiance values, and atmospheric correction was applied using the FLAASH module, configured for an urban aerosol model and mid-latitude summer atmospheric conditions. Orthogonal correction was performed using a cubic convolutional resampling method to correct geometric distortions. Image fusion was conducted using NNDiffuse Pan Sharpening to improve spatial resolution. Finally, the images were mosaicked and cropped to accurately define the study area, ensuring high fidelity and consistency of the processed images. These steps are essential to maintain the integrity and usability of the data for detailed urban structure analysis.

Landsat 8, the eighth installment in the U.S. Landsat program, is equipped with the Operational Land Imager (OLI) and the Thermal Infrared Sensor (TIRS), which provide spatial resolutions of 30 m and 100 m, respectively. This study utilizes Landsat 8 OLI\_TIRS data collected on 2 August 2021, notable for its minimal cloud coverage of 0.01%, to derive surface temperature estimates. The accuracy of these derived temperatures was assessed using the Landsat Collection 2 Level-2 product data. This product, available from the USGS (<https://www.usgs.gov/landsat-missions/landsat-collection-2-surface-temperature>, accessed on 12 September 2022), includes multispectral band surface reflectance and thermal infrared band surface temperatures, which have been processed using the enhanced Land Surface Reflectance Code (LaSRC) with an improved atmospheric correction algorithm [30]. The use of Collection 2 Level-2 data is critical in validating the accuracy of inverted surface temperatures due to its proven efficacy in surface temperature analysis [31]. This validation process ensures that the surface temperature data derived from the Landsat 8 images are robust and reliable for subsequent analyses.

## 2.3. Methodology

### 2.3.1. Reference Comparison Method

In this study, the delineation of built-up areas in Urumqi was performed using the reference comparison method, which is a widely recognized technique for processing nighttime lighting data [32]. This method involves setting various lighting thresholds and comparing the extracted built-up area results against official built-up area statistics released by the government. The optimal threshold, identified as the one that minimizes discrepancies between these datasets, was selected to ensure the robustness of the findings. Supported by quantitative analysis, this method allows the accurate delineation of built-up areas and ensures high precision and consistency in the spatial data utilized [33].

### 2.3.2. Random Forest Classification Method

For the extraction of UGS, hyperspectral data were analyzed using a supervised classification technique under ENVI 5.3 software, employing the Random Forest (RF) algorithm. This algorithm was chosen due to its proven efficacy in handling similar spectral categories [34,35], demonstrating superior performance over other classification methods.

The RF algorithm, configured to default settings with a number of trees set to 100 and the number of features determined by the square root of the total number of features, was utilized. Classification samples were meticulously selected based on visual interpretations of Google Earth and GF-2 true color imagery, ensuring the relevance and accuracy of the training data. The effectiveness of this method was quantitatively assessed, achieving an overall classification accuracy of 92.6% with a kappa coefficient of 0.82, which affirms the robustness of the classification process and validates the suitability of the data for subsequent analytical applications.

### 2.3.3. Radiative Transfer (Atmospheric Correction) Method

Currently, there are three main surface temperature inversion algorithms, with the radiative transfer method (also known as the atmospheric correction method) having an advantage over a single-channel and split-window algorithms for inversion of surface temperature [36]. The thermal infrared radiation brightness value  $L_\lambda$  received by the satellite sensor in the radiative transfer method consists of three components: the atmospheric upward radiation brightness  $L_\uparrow$ ; the energy of the real radiation brightness of the ground reaching the satellite sensor after passing through the atmosphere; and the energy  $L_\downarrow$  reflected by the atmospheric downward radiation reaching the ground. The expression of the thermal infrared radiation brightness value  $L_\lambda$  received by the satellite sensor is shown as follows (radiation transmission equation):

$$L_\lambda = [\varepsilon B(T_S) + (1 - \varepsilon)L_\downarrow]\tau + L_\uparrow \quad (1)$$

$$T_s = \frac{K_2}{\ln\left(\left(\frac{K_1}{B(T_S)}\right) + 1\right)} \quad (2)$$

where  $B$  is the Planck function;  $\varepsilon$  is the surface specific emissivity;  $\tau$  is the atmospheric transmittance in the thermal infrared band;  $T_S$  is the true surface temperature (K);  $K_1$  and  $K_2$  are the radiation constants, for TIRS Band10,  $K_1 = 774.89(\text{W}\cdot\text{m}^{-2}\cdot\text{sr}^{-1}\cdot\mu\text{m}^{-1})$ ,  $K_2 = 1321.08$  (K); TIRS Band11,  $K_1 = 480.89(\text{W}\cdot\text{m}^{-2}\cdot\text{sr}^{-1}\cdot\mu\text{m}^{-1})$ ,  $K_2 = 1201.14$  (K).

### 2.3.4. Statistical Analysis of the Sampling

In this paper, we focus on the spatial distribution of UGS and LST. So, it is necessary to determine the scale of the analysis. The sample method is an important method to study the inner city [37,38]. Therefore, 527 sample grids were obtained after a  $1 \text{ km} \times 1 \text{ km}$  grid sampling of the study area. Then, the UGS landscape metrics and mean surface temperature of each grid were extracted.

### 2.3.5. Moving Window Analysis

The moving window analysis employed FRAGSTATS 4.2 (<http://www.umass.edu/landeco/research/fragstats/fragstats.html>, accessed on 26 September 2022) software landscape metrics are sensitive to changes in scale. If the window is too small, the local characteristics of the landscape will cover the overall characteristics, and the generated image will appear to have no continuity. If the window is too large, details will be lost, and the resulting image will be blurry [39]. To avoid the increase in the spatial heterogeneity of the landscape pattern due to the unreasonable setting of the moving window size, the variation maps of landscape indices (AI, ED, PD and Shape\_am) under the corresponding windows are generated by setting different moving window edge lengths. Most of the current studies based on semi-variance function and block-base ratio in determining the analysis scale of landscape patterns assume that the variation degree of the landscape index is the same in all directions [40,41], that is, isotropic. This is followed by determining the analysis magnitude of the study area with the help of omnidirectional semi-variance function to quantitatively describe the spatial heterogeneity of the landscape pattern. A total of 735 random points were randomly generated under ArcGIS 10.4.1, and the landscape index values of the spatially randomly distributed points were extracted. GS+ 10.0 software was

used to simulate the landscape index semi-variance function under different moving window radii. This was followed by calculating the block–base ratio to analyze and determine the appropriate moving window size for the study area, and the results are shown in Figure 2.

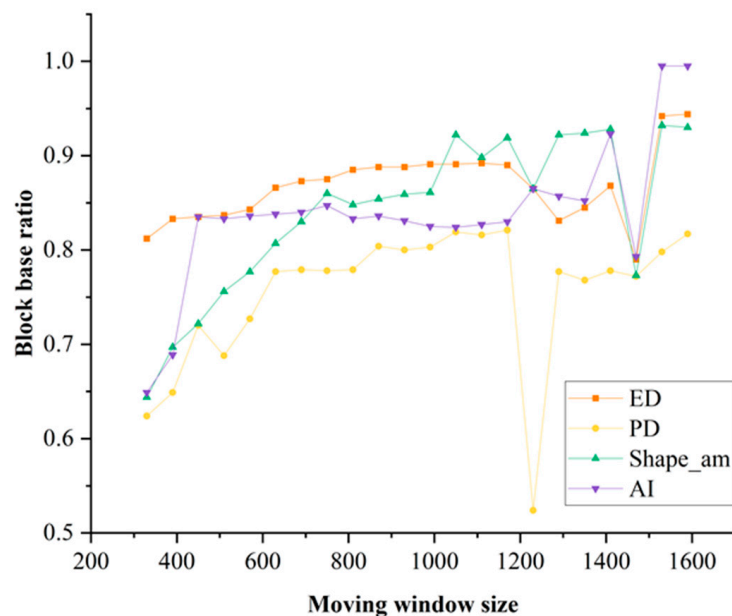


Figure 2. Spatial variation characteristics of landscape index.

In a moving window, the window is always rounded to the nearest odd cell so that the focal cell can be located in the center of the window. In this study, an odd multiple of 30 m was used as the test moving window size, which is a multiple of the resolution of Landsat 8 data. A total of 22 moving window sizes were set in intervals from 300 to 1600 m. From Figure 2, the fluctuation amplitude starts to decrease when the moving window edge length is in the interval from 810 to 990 m. Finally, 870 m was determined as the window edge length for the moving window analysis, and the shape was chosen as square, and the moving window was moved from the top left of the study area to analyze the whole study area.

### 2.3.6. Bivariate Local Indicator of Spatial Association (LISA)

The analysis in this study incorporates the bivariate local spatial autocorrelation (Bivariate Moran's I), a methodological advancement over the traditional Moran's I index for spatial autocorrelation, facilitated by GeoDa 1.18 software (<http://geodacenter.github.io/>, accessed on 28 March 2022). It extends the utility of Moran's I by enabling the examination of the correlation between a specific attribute of a spatial unit and a corresponding attribute of its neighboring units. Developed to provide deeper insights into spatial interdependencies, the Bivariate Moran's I allows a more nuanced exploration of spatial patterns by quantifying the degree of correlation between two distinct but spatially contiguous attributes [42,43], with the following equation:

$$I_{ab}^i = \frac{X_a^i - \bar{X}_a}{\sigma_a} \times \sum_{j=1}^n W_{ij} \frac{X_b^j - \bar{X}_b}{\sigma_b} \quad (3)$$

where  $x_a^i$  is the value of attribute  $a$  of cell  $i$ ;  $x_b^j$  is the value of attribute  $b$  of cell  $j$ ;  $\sigma_a$  and  $\sigma_b$  are the variances of attributes  $a$  and  $b$ , respectively.

The analysis of the spatial distribution data from regions  $i$  and  $j$  revealed distinct patterns of correlation between the independent and dependent variables, which can be categorized into four primary types of clustering including High–High (H-H), Low–Low

(L-L), High-Low (H-L), and Low-High (L-H). The H-H and L-L clusters signify a positive correlation, indicating that high values of the independent variable in region *i* are associated with high values of the dependent variable in region *j* and similarly for low-low correlations. Conversely, H-L and L-H clusters represent a negative correlation, where high values of the independent variable in one region correspond to low values of the dependent variable in another, and vice versa.

Figure 3 shows the conceptual framework of this study divided into four stages: (1) collection of data and pre-processing; (2) extraction of built-up area, UGS and inversion of urban LST; (3) spatial distribution of LST and UGS landscape indices; and (4) analyzing the relationship between the spatial distribution of LST and UGS landscape indices.

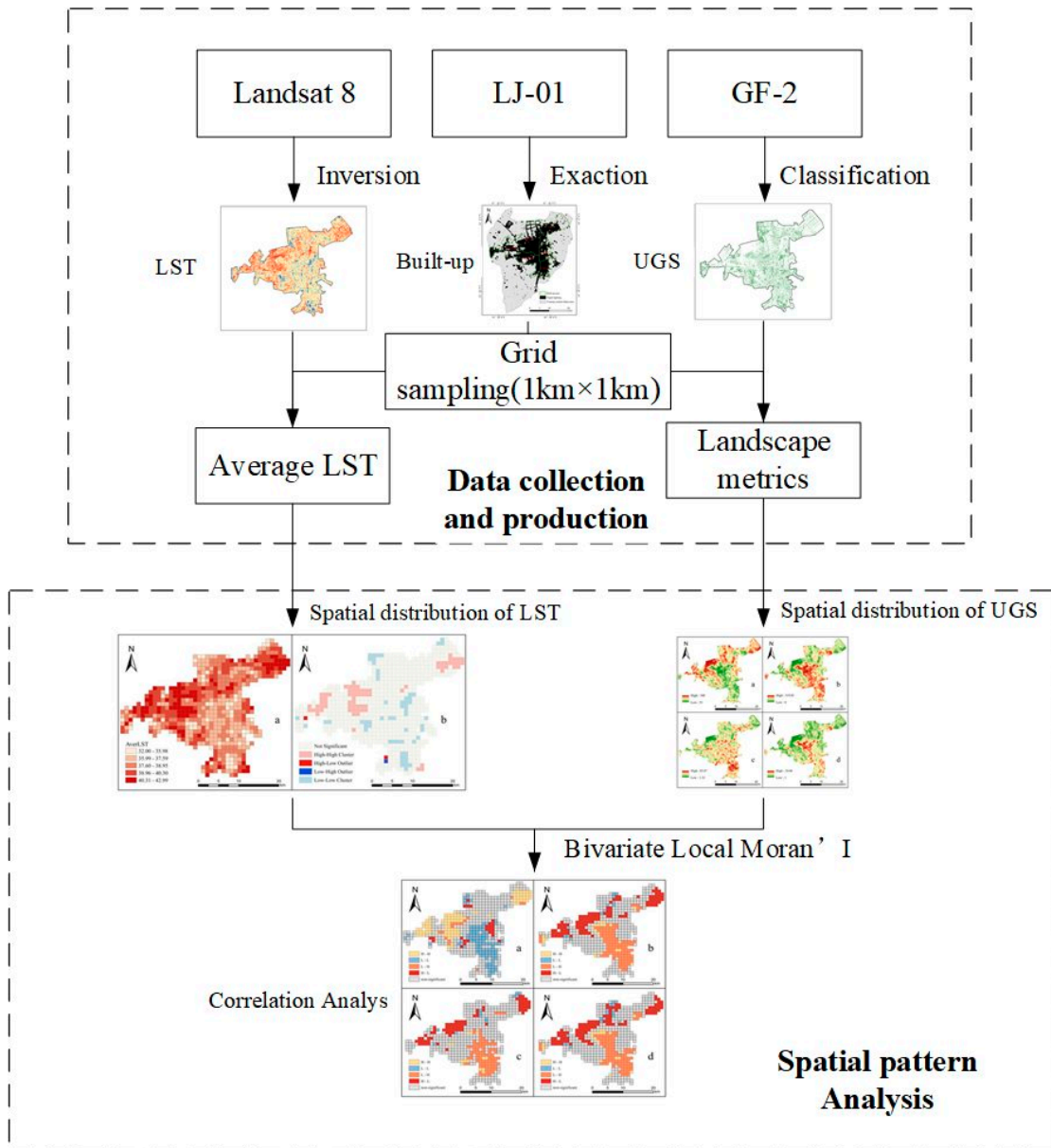


**Figure 3.** A flow chart showing the study’s conceptual framework, divided into four principal stages to be implemented in sequence.

### 3. Results

#### 3.1. Extracting Built-Up Area and UGS as Well as Inversing Land Surface Temperature

Built-up areas of Urumqi were delineated using the reference comparison method with LJ-01 satellite nighttime lighting data. This approach involved layering nighttime

lighting data from high to low intensity to align with officially announced built-up area statistics as of 15 June 2022, accessible via the Urumqi municipal website (<http://www.urumqi.gov.cn/fjbm/tjj/tjgb/509211.htm>, accessed on 14 September 2022). This method ensured accurate and current representations of urban extents. The results, depicted in Figure 4, indicate that the built-up area encompasses approximately 536.20 km<sup>2</sup>, primarily distributed across six districts including Tianshan, Saybag, Shuimogou, Xinshi, Toutunhe, and Midong.

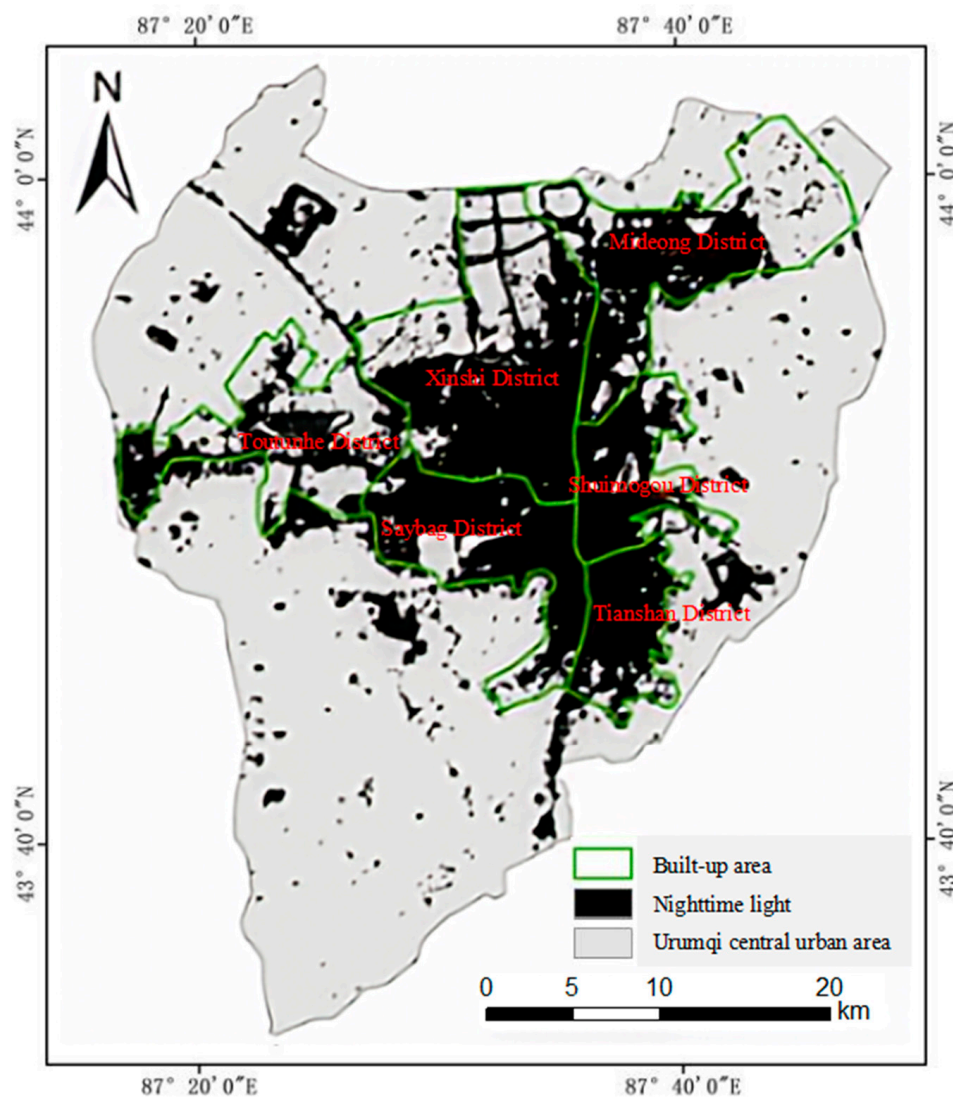


**Figure 4.** Schematic diagram of the built-up area.

Secondly, the UGS within the study area were delineated using high-resolution HMS-2 satellite imagery, as depicted in Figure 5. The map illustrates a varied distribution of UGS, with sparse coverage in the northern regions and more extensive coverage in central and southern sectors of the study area. Due to the 1 m spatial resolution of the HMS-2 imagery, which demands substantial memory for processing, it was necessary to resample these data. Therefore, Landsat imagery with a 30 m resolution was employed for resampling purposes. This resolution is acknowledged as optimal for examining the relationship between LST and landscape patterns [44]. The resampled UGS map at 30 m resolution facilitates more efficient subsequent analytical processes, ensuring the study maintains computational feasibility without compromising the spatial integrity of the environmental data.

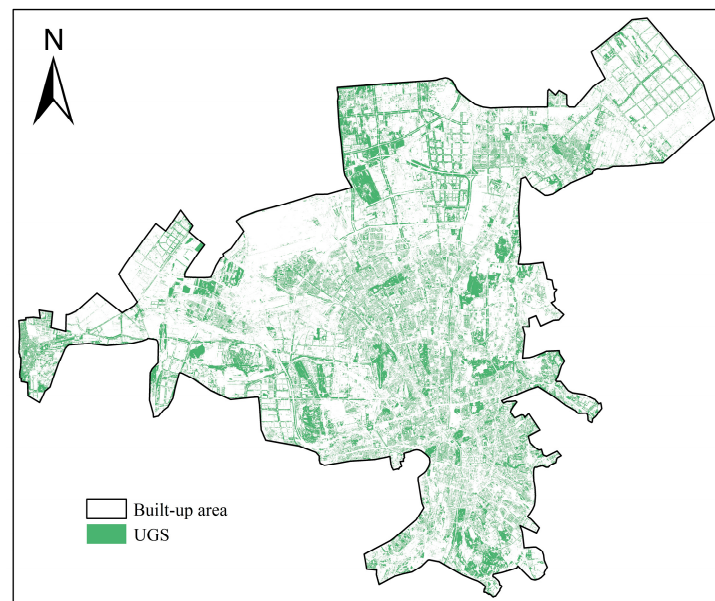


**Figure 5.** Extraction of urban green spaces (UGS) for the study area.

Surface temperature was derived using a radiative transfer method applied to Landsat 8 imagery. The inversion results, displayed in Figure 6, reveal a spatial temperature distribution with higher temperatures predominantly located in the eastern and western parts of the study area, whereas the central and southern parts exhibit lower temperatures. To ensure the reliability of these results, a rigorous validation process was conducted using Landsat Collection 2 Level-2 data. Specifically, 500 random points were selected for a comparative analysis between the surface temperatures obtained from the Landsat 8 inversion and the corresponding data from the Collection 2 Level-2 data. The analysis, visualized in Figure 7, indicated a strong correlation and alignment between the two datasets, substantiating the accuracy of the inversion process. These validated results provide a robust basis for supporting subsequent studies and analyses.

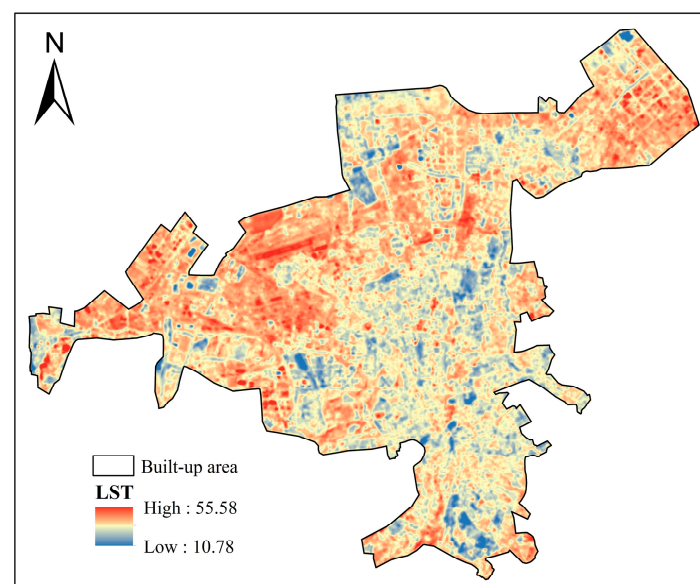


**Figure 6.** Surface temperature inversion diagram.

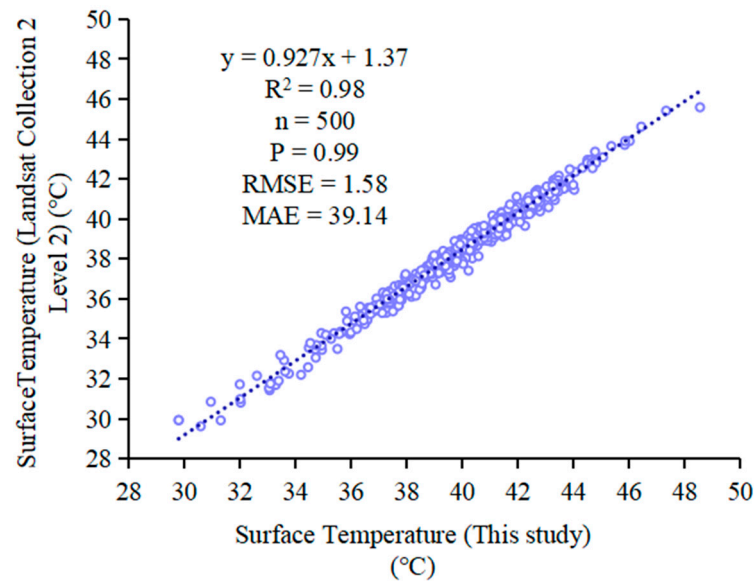


**Figure 7.** LST inversion accuracy verification.

### 3.2. Spatial Distribution of UGS Landscape Metrics

Figure 8 visualizes the distribution of four key landscape indices: AI, ED, PD, and Shape\_am, which are instrumental in analyzing UGS configuration for urban thermal environment studies.

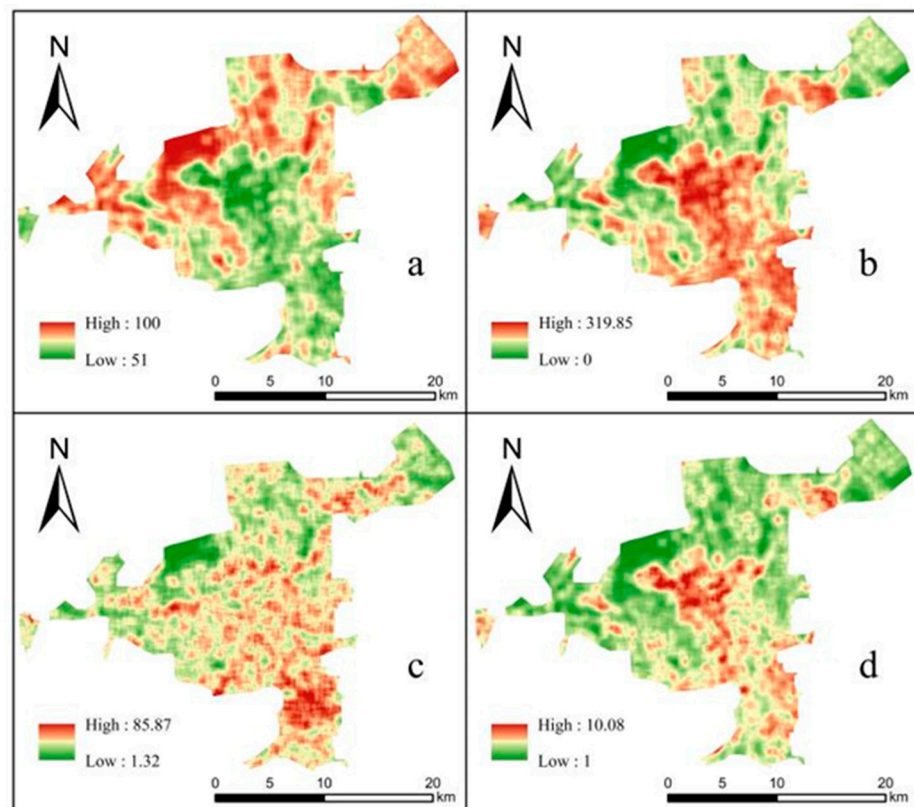


**Figure 8.** Spatial distribution of urban green space (UGS) landscape indices: (a) aggregation index (AI); (b) edge density (ED); (c) patch density (PD); and (d) area-weighted mean shape index (Shape\_am).

High aggregation values, ranging from 0.51 to 1.00, were observed in Midong, Toutunhe, and northern Xinshi, suggesting that there is a great deal of connectivity between green space, and that large, contiguous green spaces are critical for ecological corridors and

effective urban heat mitigation (Figure 8a). Lower edge densities in these areas correspond to the reduced fragmentation, supporting cohesive green infrastructure, which is advantageous for maintaining microclimatic stability and reducing edge effects that negatively impact flora and fauna by exposing them to urban environmental stresses (Figure 8b). Elevated patch densities in southern Xinshi, Saybag, Shuimogou, and Tianshan demonstrate a fragmented arrangement of green patches (Figure 8c). More irregularly shaped patches in southern Xinshi, with Shape\_am values above 1, demonstrate a complex green space structure (Figure 8d), which is in contrast to more regular and simpler green space shapes that dominate in Toutunhe and Midong. These indices collectively provide a quantitative foundation for evaluating the structural and functional characteristics of UGSs within Urumqi, supporting targeted urban planning initiatives aimed at optimizing the ecological and thermal benefits of urban green spaces.

### 3.3. Spatial Distribution of LST

Empirical studies have established a significant correlation between LST and key urban surface features, notably for impervious surfaces and vegetation cover. High-temperature areas are primarily concentrated in Midong District, Toutunhe District, and the western part of the new urban area, while low-temperature areas cluster in the southern part of the new urban area, Saybag District, Shuimogou District, and Tianshan District (Figure 9a).

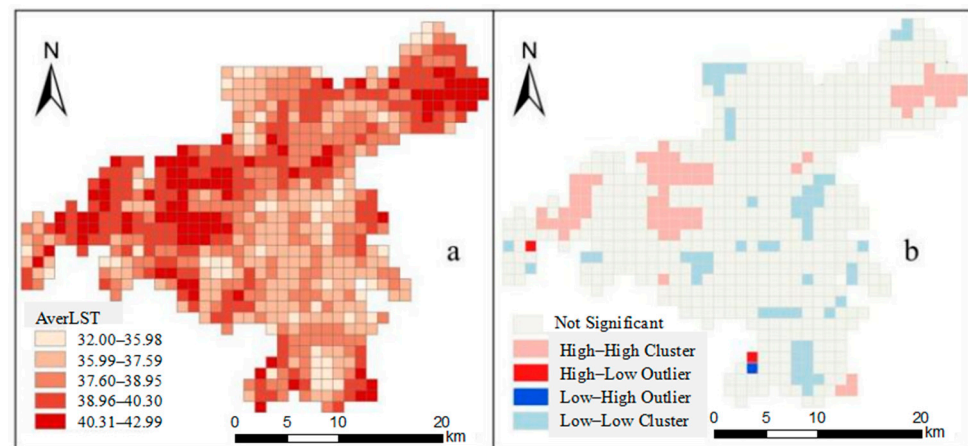


**Figure 9.** Spatial distribution of surface temperature: (a) AverLST; (b) cluster analysis.

Figure 9b shows that the high values are mainly concentrated in the western part of Xinshi District, the central part of Toutunhe District, and the eastern part of Midong District, indicating that not only their own temperature is high, but also the temperature of the adjacent units is equally high. The low values are mainly concentrated in Tianshan District, Saybag District, and Shuimogou District, with less distribution in the north and south of Xinshi District, the north of Midong District, and the west and south of Toutunhe District. The two cells with high values surrounded by low values are located in Toutunhe District and Tianshan District, indicating that these two cells are in high temperatures in spatial distribution and the cells next to them are in low-temperature conditions. The only cell with low values surrounded by high values is located in Tianshan District, indicating that this cell is at a low temperature in spatial distribution, but the cells next to it are at a high temperature. The conclusion drawn in Figure 9b coincides with Figure 9a.

### 3.4. Spatial Distribution Relationship between UGS and LST

It has been consistently indicated by previous research that an increase in UGS leads to a reduction in LST. Building on this foundation, the current study employs bivariate local spatial correlation analysis to investigate the influence of urban landscape structure indicators on regional surface temperatures, which is depicted in Figure 10.

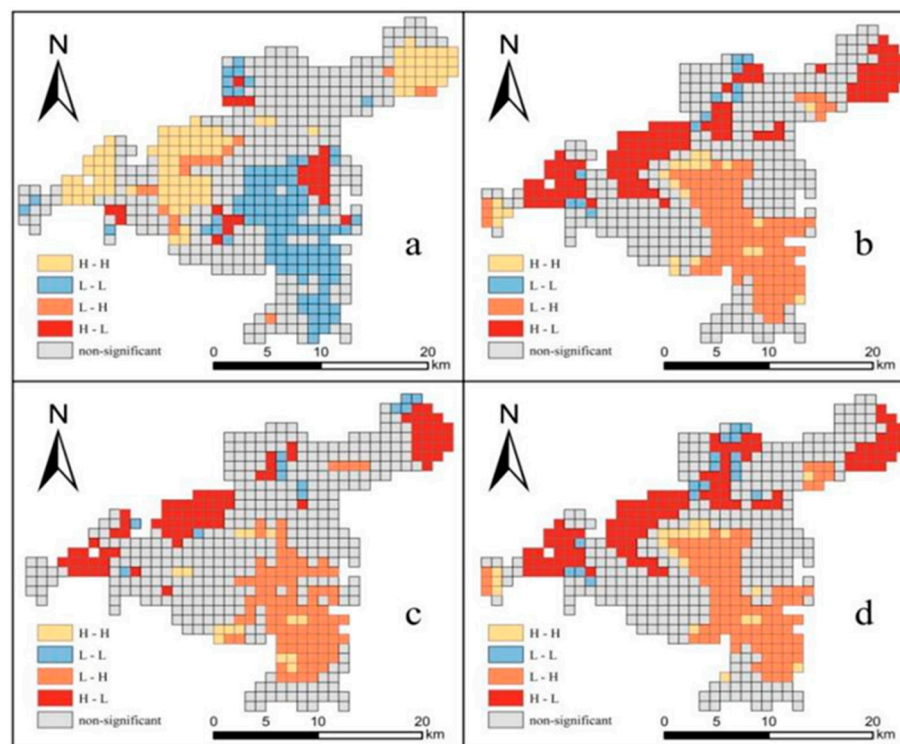


**Figure 10.** Bivariate LISA clustering diagram of UGS and LST: (a) aggregation index (AI); (b) edge density (ED); (c) patch density (PD); and (d) area-weighted mean shape index (Shape\_am).

The landscape indexes were all significantly correlated with LST to different degrees, and AI, ED, PD, and Shape\_am were all significantly correlated with LST at the 0.001 level. The results indicated that the degree of aggregation, edge density, patch density, and shape complexity index all played a role in LST. Among them, ED, PD and Shape\_am were all negatively correlated with LST, and the Moran' I index was  $-0.469$ ,  $-0.388$ , and  $-0.411$ , respectively, indicating that plaque fragmentation, UGS with a complex shape and better cooling effect, and ED had more significant effect on LST than PD. AI was positively correlated with LST, and the Moran' I index was  $0.449$ , indicating that the higher the aggregation, the higher the LST.

Based on these results, planners can logically assume that a uniform distribution of street trees within the city may be an effective way to reduce the urban heat island effect. This suggests that when planning for cities in the future with cooling benefits from UGS as an option, decision makers should focus more on the pattern of UGS rather than their number to bring maximum benefits with the same number of UGS. This is especially true for cities with severe spatial constraints due to the competing land use demands, where adding more UGS remains a major challenge.

#### 4. Discussion

##### 4.1. Policy Influence on Spatial Distribution of LST

The spatial distribution of LST in Urumqi has been notably influenced by the national planning policies, especially during the 14th Five-Year Plan period. Development was primarily focused in the Toutunhe district, potentially overlooking environmental considerations, thereby impacting the ecological balance. In contrast, traditional districts like Tianshan, Saybag, and Shuimogou have achieved an equilibrium between development and environmental benefits (thanks to mature urban planning). Notably, areas such as the Botanical Garden and Liyu Mountain Park, located in the south of the new urban area, exhibit lower average surface temperatures, underlining the cooling effects of well-planned green spaces. Conversely, the Midong District, further from the city center, exhibits higher

temperatures due to its lower population density, minimal green coverage, and proximity to industrial zones.

#### 4.2. Influence of Spatial Resolution and Landscape Metrics on LST

The relationship between the landscape metrics and LST appears to vary significantly depending on the spatial resolution of the remote sensing imagery used. For instance, ED was found to be negatively correlated with LST in studies utilizing Landsat TM imagery with a resolution of 30 m [15,45]. However, this relationship was reversed in higher resolution imagery from SPOT (10 m) and QuickBird (2.44 m), where a positive correlation between ED and LST was observed, and it intensifies with increased resolution [46]. PD has predominantly shown a negative correlation with LST, which is aligning with our findings [47]. An analysis using Sentinel 2A data to assess cooling effects in green spaces indicated a significant positive correlation between LST and PD [16]. Similarly, using GF-6 imagery and a spatial analysis grid of 1 km × 1 km, researchers found a positive correlation between PD and LST, and a negative correlation between ED, AI, and LST, which diverges from the results reported by Bao et al. [48] where AI was positively correlated with LST. A comprehensive study by Xiang et al. [49] explored the impact of various landscape metrics on LST using a 9000 m × 9000 m analysis grid. The findings indicated that AI was negatively correlated with LST, whereas PD, ED, and Shape\_am were positively correlated, utilizing land cover data at a 30 m resolution and LST data from MODIS MYDLT1D. These findings underscore the complexity of the interactions between landscape structure and LST, suggesting that spatial resolution and methodological nuances significantly influence these relationships.

#### 4.3. Methodological Considerations and Future Directions

Discrepancies observed in the correlation between landscape metrics and LST across various studies may largely stem from the differential spatial scales, at which these metrics were calculated, coupled with the inherent sensitivity of the metrics to scale changes. In our study, UGS model metrics were computed using a 1 km × 1 km grid, primarily focusing on smaller urban patches. Conversely, studies by Li et al. [46] and Xiang et al. [49] concentrating on larger UGS such as parks, often overlook the smaller patches within urban settings. This variation in scale fundamentally affects the cooling distances attributed to different UGS, thereby leading to the conflicting results noted across studies. Additionally, the significant variation in overall urban form and existing UGS patterns across different cities elucidates the observed contradictions [50]. For instance, a comprehensive assessment of urban morphology's impact on UGS models in 262 cities across China revealed that factors such as the UGS perimeter-area ratio, road density, and a composite topographic complexity index exert significant influences on landscape metrics [51]. These findings highlight the critical role that both the scale of landscape metrics and urban structural complexities play a role in influencing LST outcomes.

Recognizing several inherent limitations could impact the generalizability and precision of our findings. Firstly, the spatial resolution of the Landsat 8 data used to derive LST is relatively low (30 m for OLI and 100 m for TIRS), which may affect the granularity of our UGS and LST analysis. While this resolution is adequate for large-scale urban analysis, it might not capture finer landscape details crucial for micro-scale urban studies. To overcome this, it is recommended that future studies utilize higher-resolution satellite data, such as from the Landsat 9 mission or commercial high-resolution satellites, which can provide more detailed information and thus enhance the accuracy and reliability of the analysis. Moreover, our study's focus on a single city, Urumqi, limits the ability to generalize our findings across different urban forms and climatic regions. Urumqi's unique geographic and climatic conditions may not represent other urban environments where different UGS configurations and broader climatic factors might influence the urban heat island effect differently. To address this limitation, future research should aim to include multiple cities that vary significantly in size, climatic conditions, and urban morphology. Conducting

comparative studies across these diverse settings will help identify robust UGS evaluation indicators that are applicable under varying urban conditions. Expanding the research scope to include a broader array of urban settings will also allow for the development of generalized urban green space strategies tailored to specific climatic zones or urban configurations. This approach is crucial for devising effective urban planning and management strategies that can mitigate the urban heat island effect and contribute to climate mitigation and urban sustainability more broadly. Additionally, integrating advanced spatial analysis techniques and exploring the potential of new analytical methods, such as machine learning models that can handle complex variable interactions in large datasets, might provide deeper insights into the dynamics of UGS and LST. In conclusion, while the current study provides valuable insights into the correlation between UGS and LST in Urumqi, acknowledging and addressing these limitations through methodological enhancements and broader geographic studies will greatly enhance the reliability and applicability of future urban ecological research.

## 5. Conclusions

The degradation of urban environmental quality, evidenced by deteriorating air quality and increasing UHI effects, is one of the adverse consequences of uncontrolled urbanization. Nonetheless, these negative effects can be mitigated. Urban vegetation plays a pivotal role in preserving the ecological equilibrium within cities, with the ecological services offered by UGS exhibiting notable diversity across varying landscape configurations. Consequently, this study analyzed the spatial distribution characteristics of UGS and LST in Urumqi, situated in an arid zone, and explored the bivariate local spatial autocorrelation between UGS distribution and LST as a reference for urban planners to design UGS scientifically. The following conclusions are drawn from the results of this study:

- (1) Patches with a high aggregation index are predominantly located in the study area of Midong District, Toutunhe District, and the northern part of Xinshi District, whereas the distribution of edge density contrasts with that of the aggregation index. The southern part of Xinshi District, Saybag District, Shuimogou District, and Tianshan District exhibit higher densities of patches, with Xinshi District encompassing the largest distribution area of UGS, albeit non-uniformly distributed.
- (2) The high-temperature zones are primarily concentrated in Midong District, Toutunhe District, and the western part of Xinshi District, while the low-temperature zones predominantly cluster in the southern part of Xinshi District, Saybag District, Shuimogou District, and Tianshan District.
- (3) AI, ED, PD, and Shape\_am were all found to be significantly correlated with LST at the 0.001 level. Conversely, ED, PD, and Shape\_am exhibited negative correlations with LST, while AI was positively correlated with LST.

This study provides a more scientific reference for urban planners to evaluate UGS by studying the influence of different landscape metrics of UGS on LST. However, further studies and in-depth exploration of different cities are needed to reveal the impact of the UGS model.

**Author Contributions:** Conceptualization, M.Z.; methodology, M.Z. and J.W.; formal analysis, M.Z.; resources, F.Z.; data curation, M.Z.; writing—original draft, M.Z.; visualization, M.Z.; supervision, F.Z.; funding acquisition, F.Z. All authors have read and agreed to the published version of the manuscript.

**Funding:** This research was supported by the Strategic Priority Program of the Chinese Academy of Sciences, Pan-Third Pole Environment Study for a Green Silk Road (XDA20040400), and the Tianshan Talent Project (Phase III) of the Xinjiang Uygur Autonomous region, China.

**Data Availability Statement:** The datasets used and analyzed during the current study are available from the corresponding author on reasonable request.

**Acknowledgments:** The authors would like to thank Cheng Chen of Zhejiang Normal University, Daosheng Chen of Xinjiang University, Ngai Weng Chan and Mou Leong Tan of Universiti Sains Malaysia, Jinchao Shi of the University of Memphis, and Cheng Li of Yangzhou University for reviewed and improved our paper.

**Conflicts of Interest:** The authors declare no competing interests.

## References

- Vaidya, H.; Chatterji, T. SDG 11 sustainable cities and communities: SDG 11 and the new urban agenda: Global sustainability frameworks for local action. In *Actioning the Global Goals for Local Impact: Towards Sustainability Science, Policy, Education and Practice*; Springer: Singapore, 2020; pp. 173–185.
- Xue, B.; Han, B.; Li, H.; Gou, X.; Yang, H.; Thomas, H.; Stückrad, S. Understanding ecological civilization in China: From political context to science. *Ambio* **2023**, *52*, 1895–1909. [[CrossRef](#)] [[PubMed](#)]
- Ngom, R.; Gosselin, P.; Blais, C. Reduction of disparities in access to green spaces: Their geographic insertion and recreational functions matter. *Appl. Geogr.* **2016**, *66*, 35–51. [[CrossRef](#)]
- Corburn, J. Cities, climate change and urban heat island mitigation: Localising global environmental science. *Urban Stud.* **2009**, *46*, 413–427. [[CrossRef](#)]
- Arnfield, A. Two decades of urban climate research: A review of turbulence, exchanges of energy and water, and the urban heat island. *Int. J. Climatol. J. R. Meteorol. Soc.* **2003**, *23*, 1–26. [[CrossRef](#)]
- Li, X.; Zhou, W.; Ouyang, Z.; Xu, W.; Zheng, H. Spatial pattern of greenspace affects land surface temperature: Evidence from the heavily urbanized Beijing metropolitan area, China. *Landsc. Ecol.* **2012**, *27*, 887–898. [[CrossRef](#)]
- Ke, X.; Men, H.; Zhou, T.; Li, Z.; Zhu, F. Variance of the impact of urban green space on the urban heat island effect among different urban functional zones: A case study in Wuhan. *Urban For. Urban Green* **2021**, *62*, 127159. [[CrossRef](#)]
- Wang, X.; Meng, Q.; Zhang, L.; Hu, D. Evaluation of urban green space in terms of thermal environmental benefits using geographical detector analysis. *Int. J. Appl. Earth Obs. Geoinf.* **2021**, *105*, 102610. [[CrossRef](#)]
- Chan, N.; Tan, M.; Ghani, A.; Zakaria, N. Sustainable urban drainage as a viable measure of coping with heat and floods due to climate change. *IOP Conf. Ser. Earth Environ. Sci.* **2019**, *257*, 012013. [[CrossRef](#)]
- Aram, F.; García, E.H.; Solgi, E.; Mansournia, S. Urban green space cooling effect in cities. *Heliyon* **2019**, *5*, e01339. [[CrossRef](#)]
- Masoudi, M.; Tan, P.; Fadaei, M. The effects of land use on spatial pattern of urban green spaces and their cooling ability. *Urban Clim.* **2021**, *35*, 100743. [[CrossRef](#)]
- Shah, A.; Garg, A.; Mishra, V. Quantifying the local cooling effects of urban green spaces: Evidence from Bengaluru, India. *Landsc. Urban Plan.* **2021**, *209*, 104043. [[CrossRef](#)]
- Zhou, W.; Cao, W.; Wu, T.; Zhang, T. The win-win interaction between integrated blue and green space on urban cooling. *Sci. Total Environ.* **2023**, *863*, 160712. [[CrossRef](#)] [[PubMed](#)]
- Proutsos, N.; Tigkas, D.; Tsevreni, I.; Alexandris, S.; Solomou, A.; Bourletsikas, A.; Stefanidis, S.; Nwokolo, S. A thorough evaluation of 127 potential evapotranspiration models in two mediterranean urban green sites. *Remote Sens.* **2023**, *15*, 3680. [[CrossRef](#)]
- Maimaitiyiming, M.; Ghulam, A.; Tiyyip, T.; Pla, F.; Latorre-Carmona, P.; Halik, Ü.; Sawut, M.; Caetano, M. Effects of green space spatial pattern on land surface temperature: Implications for sustainable urban planning and climate change adaptation. *ISPRS J. Photogramm. Remote Sens.* **2014**, *89*, 59–66. [[CrossRef](#)]
- Pramanik, S.; Punia, M. Environment. Assessment of green space cooling effects in dense urban landscape: A case study of Delhi, India. *Model. Earth Syst. Environ.* **2019**, *5*, 867–884. [[CrossRef](#)]
- Guo, L.; Liu, R.; Men, C.; Wang, Q.; Miao, Y.; Zhang, Y. Quantifying and simulating landscape composition and pattern impacts on land surface temperature: A decadal study of the rapidly urbanizing city of Beijing, China. *Sci. Total Environ.* **2019**, *654*, 430–440. [[CrossRef](#)] [[PubMed](#)]
- Rakoto, P.; Deilami, K.; Hurley, J.; Amati, M.; Sun, Q.; Greening, U. Revisiting the cooling effects of urban greening: Planning implications of vegetation types and spatial configuration. *Urban For. Urban Green.* **2021**, *64*, 127266. [[CrossRef](#)]
- Yuan, B.; Zhou, L.; Hu, F.; Wei, C. Effects of 2D/3D urban morphology on land surface temperature: Contribution, response, and interaction. *Urban Clim.* **2024**, *53*, 101791. [[CrossRef](#)]
- Huang, S.; Xiao, X.; Tian, T.; Che, Y. Seasonal influences on preferences for urban blue-green spaces: Integrating land surface temperature into the assessment of cultural ecosystem service value. *Sustain. Cities Soc.* **2024**, *102*, 105237. [[CrossRef](#)]
- Kumar, B.; Anusha, B.; Babu, k.; Sree, P. Identification of climate change impact and thermal comfort zones in semi-arid regions of AP, India using LST and NDBI techniques. *J. Clean. Prod.* **2023**, *407*, 137175. [[CrossRef](#)]
- Cheng, Y.; Wang, W.; Ren, Z.; Zhao, Y.; Liao, Y.; Ge, Y.; Wang, J.; He, J.; Gu, Y.; Wang, Y.; et al. Multi-scale Feature Fusion and Transformer Network for urban green space segmentation from high-resolution remote sensing images. *Int. J. Appl. Earth Obs. Geoinf.* **2023**, *124*, 103514. [[CrossRef](#)]
- Guan, J.; Wang, R.; Berkel, D.; Liang, Z. How spatial patterns affect urban green space equity at different equity levels: A bayesian quantile regression approach. *Landsc. Urban Plan.* **2023**, *233*, 104709. [[CrossRef](#)]

24. Connors, J.; Galletti, C.; Chow, W. Landscape configuration and urban heat island effects: Assessing the relationship between landscape characteristics and land surface temperature in Phoenix, Arizona. *Landscape Ecol.* **2013**, *28*, 271–283. [[CrossRef](#)]
25. El-Beltagy, A.; Madkour, M. Impact of climate change on arid lands agriculture. *Agric. Food Secur.* **2012**, *1*, 3. [[CrossRef](#)]
26. Chen, D.; Zhang, F.; Zhang, M.; Meng, Q.; Jim, C.Y.; Shi, J.; Tan, M.L.; Ma, X. Landscape and vegetation traits of urban green space can predict local surface temperature. *Sci. Total Environ.* **2022**, *825*, 154006. [[CrossRef](#)] [[PubMed](#)]
27. Li, X.; Zhao, L.; Li, D.; Xu, H. Mapping urban extent using Luojia 1-01 nighttime light imagery. *Sensors* **2018**, *18*, 3665. [[CrossRef](#)] [[PubMed](#)]
28. Yun, C. GF-2 satellite. *Satell. Appl.* **2014**, *9*, 65. (In Chinese)
29. Wang, X.; Meng, Q.; Zhao, S.; Li, J.; Zhang, L.; Chen, X. Urban green space classification and landscape pattern measurement based on GF-2 image. *J. Geoinf. Sci.* **2020**, *22*, 1971–1982.
30. Duan, S.; Ru, C.; Li, Z.; Wang, M.; Xu, H.; Li, H.; Wu, P.; Zhan, W.; Zhou, J.; Zhao, W. Reviews of methods for land surface temperature retrieval from Landsat thermal infrared data. *Natl. Remote Sens. Bull.* **2021**, *25*, 1591–1617. [[CrossRef](#)]
31. Onáčillová, K.; Gallay, M.; Paluba, D.; Péliová, A.; Tokarčík, O.; Laubertová, D. Combining landsat 8 and sentinel-2 data in google earth engine to derive higher resolution land surface temperature maps in urban environment. *Remote Sens.* **2022**, *14*, 4076. [[CrossRef](#)]
32. Zhang, M.; Zhang, F.; Chen, D.; Tan, M.L.; Chan, N. Urban local surface temperature prediction using the urban gray-green space landscape and vegetation indices. *Build. Environ.* **2022**, *226*, 109723. [[CrossRef](#)]
33. Li, G.; Fan, J.; Zhou, Y.; Zhang, Y. Development characteristics estimation of Shandong peninsula urban agglomeration using VIIRS night light data. *Remote Sens. Technol. Appl.* **2020**, *35*, 1348–1359.
34. Naidoo, L.; Cho, M.A.; Mathieu, R.; Asner, G. Classification of savanna tree species, in the Greater Kruger National Park region, by integrating hyperspectral and LiDAR data in a Random Forest data mining environment. *ISPRS J. Photogramm. Remote Sens.* **2012**, *69*, 167–179. [[CrossRef](#)]
35. Pu, R.; Landry, S.; Yu, Q. Assessing the potential of multi-seasonal high resolution Pléiades satellite imagery for mapping urban tree species. *Int. J. Appl. Earth Obs. Geoinf.* **2018**, *71*, 144–158.
36. Liu, H.; Weng, Q. Scaling effect on the relationship between landscape pattern and land surface temperature. *Photogramm. Eng. Remote Sens.* **2009**, *75*, 291–304. [[CrossRef](#)]
37. Yu, X.; Guo, X.; Wu, Z. Land surface temperature retrieval from Landsat 8 TIRS—Comparison between radiative transfer equation-based method, split window algorithm and single channel method. *Remote Sens.* **2014**, *6*, 9829–9852. [[CrossRef](#)]
38. Mutani, G.; Todeschi, V. Roof-integrated green technologies, energy saving and outdoor thermal comfort: Insights from a case study in urban environment. *Int. J. Sustain. Dev. Plan.* **2021**, *16*, 13–23. [[CrossRef](#)]
39. Vega, K.A.; Küffer, C. Promoting wildflower biodiversity in dense and green cities: The important role of small vegetation patches. *Urban For. Urban Green.* **2021**, *62*, 127165. [[CrossRef](#)]
40. McGarigal, K. *FRAGSTATS Help*; University of Massachusetts: Amherst, MA, USA, 2015; 182p.
41. Mou, Y.; Chen, Q.; Li, L.; Tu, C.; Lu, X. Spatial differentiation and influencing factors of surface soil selenium in Huaxi District, Guiyang. *Acta Sci. Circumstantiae* **2022**, *42*, 415–424. (In Chinese)
42. Song, S.; Wang, Y.; Shi, M.; Hu, S.; Xu, D. Effects of landscape pattern type on soil erosion. *Soil Water Conserv. Res.* **2022**, *29*, 85–92. (In Chinese)
43. Gutiérrez, J.; García-Palomares, J.C.; Romanillos, G.; Salas-Olmedo, M. The eruption of Airbnb in tourist cities: Comparing spatial patterns of hotels and peer-to-peer accommodation in Barcelona. *Tour. Manag.* **2017**, *62*, 278–291. [[CrossRef](#)]
44. Yao, X.; Zeng, J.; Li, W. Spatial correlation characteristics of urbanization and land ecosystem service value in Wuhan Urban Agglomeration. *Trans. Chin. Soc. Agric. Eng.* **2015**, *31*, 249–256.
45. Li, B.; Shi, X.; Wang, H.; Qin, M. Analysis of the relationship between urban landscape patterns and thermal environment: A case study of Zhengzhou City, China. *Environ. Monit. Assess.* **2020**, *192*, 540. [[CrossRef](#)] [[PubMed](#)]
46. Li, X.; Zhou, W.; Ouyang, Z. Relationship between land surface temperature and spatial pattern of greenspace: What are the effects of spatial resolution? *Landscape Urban Plan.* **2013**, *114*, 1–8. [[CrossRef](#)]
47. Li, J.; Song, C.; Cao, L.; Zhu, F.; Meng, X.; Wu, J. Impacts of landscape structure on surface urban heat islands: A case study of Shanghai, China. *Remote Sens. Environ.* **2011**, *115*, 3249–3263. [[CrossRef](#)]
48. Bao, T.; Li, X.; Zhang, J.; Zhang, Y.; Tian, S. Assessing the distribution of urban green spaces and its anisotropic cooling distance on urban heat island pattern in Baotou, China. *ISPRS Int. J. Geo-Inf.* **2016**, *5*, 12. [[CrossRef](#)]
49. Xiang, Y.; Ye, Y.; Peng, C.; Teng, M.; Zhou, Z. Seasonal variations for combined effects of landscape metrics on land surface temperature (LST) and aerosol optical depth (AOD). *Ecol. Indic.* **2022**, *138*, 108810. [[CrossRef](#)]
50. Huang, J.; Lu, X.; Sellers, J. A global comparative analysis of urban form: Applying spatial metrics and remote sensing. *Landscape Urban Plan.* **2007**, *82*, 184–197. [[CrossRef](#)]
51. Huang, C.; Yang, J.; Jiang, P. Assessing impacts of urban form on landscape structure of urban green spaces in China using Landsat images based on Google Earth Engine. *Remote Sens.* **2018**, *10*, 1569. [[CrossRef](#)]

**Disclaimer/Publisher’s Note:** The statements, opinions and data contained in all publications are solely those of the individual author(s) and contributor(s) and not of MDPI and/or the editor(s). MDPI and/or the editor(s) disclaim responsibility for any injury to people or property resulting from any ideas, methods, instructions or products referred to in the content.